Berry-Curvature Engineering for Nonreciprocal Directional Dichroism in Two-Dimensional Antiferromagnets

Wenhao Liang,[1] Junjie Zeng,[2] Zhenhua Qiao,[1,3,*] Yang Gao,[1,3,†] and Qian Niu[1]
[1]International Centre for Quantum Design of Functional Materials, CAS Key Laboratory of Strongly-Coupled Quantum Matter Physics, and Department of Physics, University of Science and Technology of China, Hefei, Anhui 230026, China
[2]Institute for Structure and Function, Department of Physics, and Chongqing Key Laboratory for Strongly Coupled Physics, Chongqing University, Chongqing 400044, China
[3]Hefei National Laboratory, University of Science and Technology of China, Hefei 230088, China

(Received 12 June 2023; revised 2 October 2023; accepted 17 November 2023; published 21 December 2023)

In two-dimensional antiferromagnets, we find that the mixed Berry curvature can be attributed as the geometrical origin of the nonreciprocal directional dichroism (NDD), which refers to the difference in light absorption between opposite propagation directions. This Berry curvature is closely related to the uniaxial strain in accordance with the symmetry constraint, leading to a highly tunable NDD, whose sign and strength can be tuned via strain direction. We choose the lattice model of $MnBi_2Te_4$ as a concrete example. The coupling between mixed Berry curvature and strain also suggests the magnetic quadrupole of the Bloch wave packet as the macroscopic order parameter probed by the NDD in two dimensions, which is distinct from the multiferroic order $\boldsymbol{P}\times\boldsymbol{M}$ or the spin toroidal and quadrupole order within a unit cell in previous studies. Our work paves the way for the Berry-curvature engineering for optical nonreciprocity in two-dimensional antiferromagnets.

DOI: 10.1103/PhysRevLett.131.256901

Antiferromagnetism in two dimensions has attracted growing interest in recent years [1–8]. Benefiting from both the ultrafast dynamics and absence of stray fields from antiferromagnetism [5], and remarkable tunability in two-dimensional van der Waals structures [9–12], two-dimensional antiferromagnets can play an essential role in designing next-generation spintronic devices [5–8]. Their connection with topological and geometrical physics is also recognized [13–20]. This naturally integrates spintronics with topological protection as well as a distinct tuning scheme via Berry-curvature engineering. One fundamental and timely question to answer in this regard is how the geometrical quantity (e.g., Berry curvature) is intertwined with various degrees of freedom, such as charge, spin, and lattice. One example is the layer Hall effect in the antiferromagnetic $MnBi_2Te_4$ system due to locking of Berry curvature with different layers [20]. Hereinbelow, we investigate the coupling between Berry curvature and uniaxial strain through the nonreciprocal directional dichroism (NDD).

NDD refers to the difference in optical absorption between counterpropagating lights with linear polarization [21–37]. It originates from the dynamical magnetoelectric coupling [26–33] and has a deep connection with both the order parameter and geometrical property of Bloch electrons. Per symmetry consideration, NDD requires the breaking of time-reversal symmetry ($\mathcal{T}$) and inversion symmetry ($\mathcal{I}$), and is insensitive to the combined $\mathcal{TI}$ symmetry. In three dimensions, such symmetry requirements are generally associated with two types of order parameters, i.e., the multiferroic order $\boldsymbol{P}\times\boldsymbol{M}$ [25–33] ($\boldsymbol{P}$ is the electrical polarization and $\boldsymbol{M}$ the magnetization) and antiferromagnetism [34–37]. To be precise, in the latter case, the local spin arrangement within a unit cell should possess a spin toroidal order $\boldsymbol{t}\propto\sum_n \boldsymbol{r}_n\times\boldsymbol{s}_n$ or a symmetric spin quadrupole order $q^s_{ij}\propto\sum_n[r_{ni}s_{nj}+r_{nj}s_{ni}-\frac{2}{3}\delta_{ij}\boldsymbol{r}_n\cdot\boldsymbol{s}_n]$ [38], where $\boldsymbol{r}_n$ and $\boldsymbol{s}_n$ label the position and spin at lattice site n, respectively. Such secondary order parameters then couple with the propagation direction of light, leading to the NDD. On the microscopic level, based on the band theory analysis in three dimensions, the geometrical origin of NDD is the quantum metric dipole of the Bloch state [22], which brings unique peak structures.

In this Letter, we generalize the microscopic theory of NDD to two-dimensional antiferromagnets. We identify the Berry curvature in the mixed parameter space $(\boldsymbol{k},\tilde{\boldsymbol{B}})$ as the geometrical origin, instead of the quantum metric dipole for the three-dimensional counterpart. More importantly, in the lattice model of $MnBi_2Te_4$, we find that the Berry curvature exhibits hot regions near the Γ point, whose shape is closely tied to the uniaxial strain. Therefore, the strength and sign of the NDD can be manipulated by the strain direction.

The coupling between Berry curvature and uniaxial strain also reveals a distinct mechanism for the NDD. With strain, $\boldsymbol{P}\times\boldsymbol{M}$ always vanishes due to the combined $\mathcal{TI}$ symmetry; the spin toroidal order $\boldsymbol{t}$ is also zero, and the

quadrupole order q^s_{ij} remains unchanged. Therefore, none of them are responsible for the NDD, which strongly depends on the strain. We then identify the magnetic quadrupole $\mathcal{Q}_{ij}$ of the wave packet as the macroscopic order parameter behind the NDD, whose microscopic expression contains the mixed Berry curvature as well. Utilizing the close relation between mixed Berry curvature and strain, we find that the NDD depends linearly on $\mathcal{Q}_{ij}$. Therefore, the NDD can probe two-dimensional antiferromagnetism via $\mathcal{Q}_{ij}$.

Geometrical origin of NDD in two dimensions.—We first sketch the microscopic theory of NDD in two dimensions. Without loss of generality, we assume that a light, linearly polarized along the x direction and propagating along the z direction, is normally incident on a bilayer antiferromagnet. The multilayer case can be obtained straightforwardly [39]. The general form of the light-induced current can then be expressed as

$$J_x(\omega) = \sigma_{xx}(\omega)E_x(\omega) + \sigma_{xxz}(\omega)q_z E_x(\omega), \tag{1}$$

with ω and q_z being the frequency and wave vector of the light, respectively. $\sigma_{xx}(\omega)$ is the usual optical conductivity, and $\sigma_{xxz}(\omega)$ corresponds to NDD, as the resulting current flips sign with the flipping of the light propagation direction, i.e., q_z. In three dimensions, $\sigma_{xxz}(\omega)$ can be evaluated by considering the energy and momentum transfer during the optical transition. However, the momentum transfer cannot be directly implemented in two dimensions due to the loss of the translational symmetry along the thickness direction.

Following the treatment in Ref. [40], we note that the coupling between the electron in the bilayer antiferromagnet and the light vector potential $A_x = A_0 e^{i(q_z z-\omega t)}$ ($z = \pm d$ for the top and bottom layers) can be put in the form $\hat{H}' = -\hat{J}_x \cdot A_0 e^{-i\omega t} - 2m_y B_y$ [39], where $\hat{J}_x = -e\hat{v}_x$ is the current operator, $B_y = iq_z A_0 e^{-i\omega t}$ is the magnetic field sensed by the bilayer antiferromagnet, and $\hat{m}_y = (d/2)(\hat{J}_{1x} - \hat{J}_{2x})$ is the magnetic moment operator with $2d$, $\hat{J}_{1x}$, and $\hat{J}_{2x}$ being the thickness, and the current operator in the top and bottom layers, respectively. This coupling is given to the first order in both A_0 and q_z.

Based on the above light-electron interaction, we adopt the linear response theory to derive $\sigma_{xxz}(\omega)$. It contains two contributions: the current in response to B_y and the magnetization in response to E_x. To be compact, we introduce an auxiliary constant magnetic field $\tilde{B}_y$ along the y direction, such that the Hamiltonian without light irradiation reads $\hat{H} = \hat{H}_0 - 2m_y\tilde{B}_y$, which recovers the original unperturbed Hamiltonian $\hat{H}_0$ in the limit of $\tilde{B}_y \to 0$. $\sigma_{xxz}(\omega)$ can then read as [39]

$$\sigma_{xxz}(\omega) = \frac{2ie}{\hbar\omega}\sum_{mn}\int\frac{d\boldsymbol{k}}{(2\pi)^2}\frac{f_{mn}\varepsilon^2_{mn}}{\varepsilon_{mn}+\hbar\omega+i\eta}\Omega^{nm}_{k_x,\tilde{B}_y}|_{\tilde{B}_y\to 0}, \tag{2}$$

where $f_{mn} = f_m - f_n$ with f_n being the Fermi distribution function for band n, $\varepsilon_{mn} = \varepsilon_m - \varepsilon_n$ with ε_n being the energy dispersion for band n, and $\eta \to 0^+$. $\Omega^{nm}_{k_x,\tilde{B}_y}$ is the Berry curvature in the mixed space $(\boldsymbol{k}, \tilde{\boldsymbol{B}})$ for a pair of bands n, m:

$$\Omega^{nm}_{k_x,\tilde{B}_y} = 2\mathrm{Im}\big(\langle m\boldsymbol{k}|\partial_{k_x}|n\boldsymbol{k}\rangle\langle n\boldsymbol{k}|\partial_{\tilde{B}_y}|m\boldsymbol{k}\rangle\big), \tag{3}$$

where $|n\boldsymbol{k}\rangle$ is the periodic part of the Bloch state in band n for the Hamiltonian $\hat{H}$. Equation (2) can be straightforwardly generalized to multilayer systems that are amenable for first-principles calculations [39].

In Eq. (2), the key geometrical quantity is the mixed Berry curvature. To further illuminate its physical and geometrical meaning, several comments are in order. First, we emphasize that $\Omega^{nm}_{k_x,\tilde{B}_y}$ is defined for a pair of bands instead of the usual Berry curvature for a single band. This is a characteristic feature in optics as the optical transition always involves a pair of bands. $\Omega^{nm}_{k_x,\tilde{B}_y}$ thus characterizes the geometrical feature of such an optical transition. The relation between $\Omega^{nm}_{k_x,\tilde{B}_y}$ and NDD can be further illuminated by considering the oscillator strength of the optical transition [53]

$$f_{n\to m}(q_z) = \frac{2m_e}{e\hbar\omega_{mn}}|\langle m\boldsymbol{k}|\hat{J}_x + 2iq_z\hat{m}_y|n\boldsymbol{k}\rangle|^2. \tag{4}$$

We then find that [39]

$$f_{n\to m}(q_z) - f_{n\to m}(-q_z) = 8q_z m_e\omega_{mn}\Omega^{nm}_{k_x,\tilde{B}_y}|_{\tilde{B}_y\to 0}. \tag{5}$$

Therefore, a nonzero mixed Berry curvature necessarily makes the electron respond differently for counterpropagating lights.

Second, $\Omega^{nm}_{k_x,\tilde{B}_y}$ can be viewed as the interband Berry curvature [54]. By summing over band index m, we obtain $\Omega^{n}_{k_x,\tilde{B}_y} = \sum_m \Omega^{nm}_{k_x,\tilde{B}_y}$. Here, $\Omega^{n}_{k_x,\tilde{B}_y}$ is the familiar Berry curvature in a parameter space $(\boldsymbol{k}, \tilde{\boldsymbol{B}})$ for a single band n, and it can be expressed using the Berry connection: $\Omega^{n}_{k_x,\tilde{B}_y} = \partial_{k_x}A^n_{\tilde{B}_y} - \partial_{\tilde{B}_y}A^n_{k_x}$ with $A^n_\xi = \langle n\boldsymbol{k}|i\partial_\xi|n\boldsymbol{k}\rangle$ being the Berry connection for band n and $\xi = k_x$ or $\tilde{B}_y$. It should be noted that $\Omega^{nm}_{k_x,\tilde{B}_y}$ coincides with the familiar Berry curvature if the system only consists of two bands. The total mixed Berry curvature for the ground state is an intrinsic bulk property of Bloch bands and can be obtained from the optical sum rule. We get that [39]

$$\int_0^\infty\frac{\mathrm{Re}[\sigma_{xxz}(\omega)]}{\omega}d\omega = -4\pi e\hbar\sum_{n\in\mathrm{occ}}\int\frac{d\boldsymbol{k}}{(2\pi)^2}\Omega^{n}_{k_x,\tilde{B}_y}|_{\tilde{B}_y\to 0}, \tag{6}$$

where "occ" means occupied band indices.

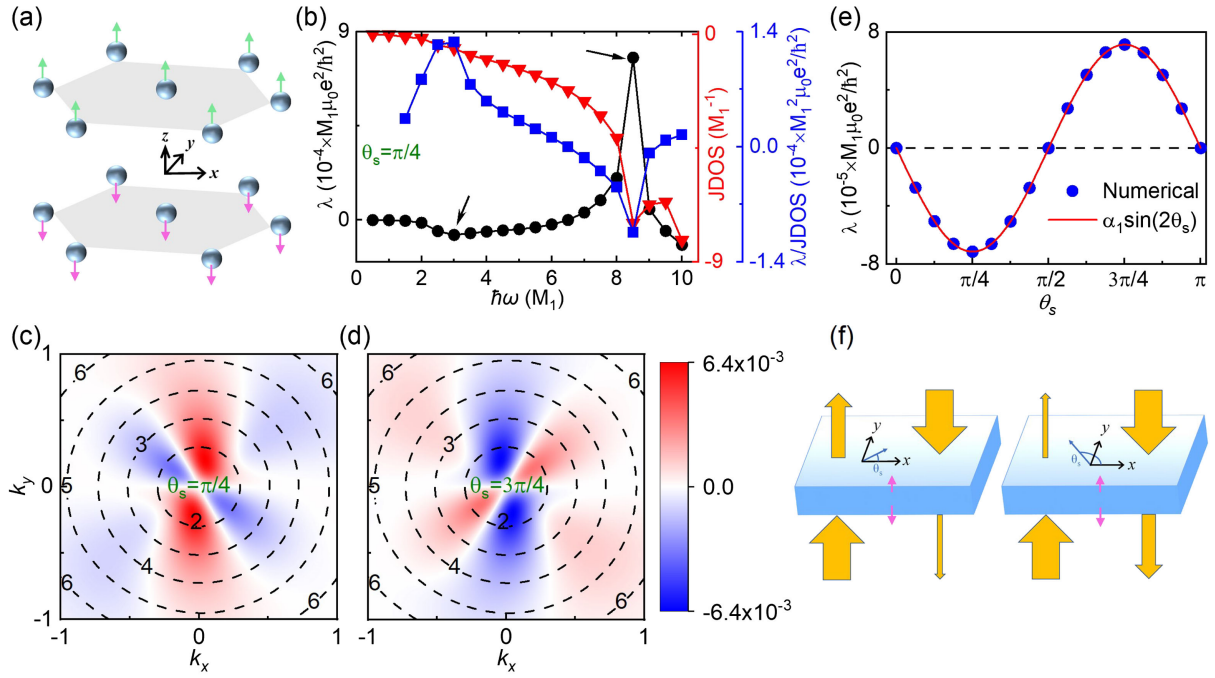

FIG. 1. Strain-tunable NDD in bilayer $MnBi_2Te_4$. (a) The lattice structure. (b) λ [$\lambda = (\chi/2d)$], joint density of states (JDOS), and λ/JDOS with a strain angle $\theta_s = \pi/4$. (c),(d) The mixed Berry curvature $\Omega^{nm}_{k_x,\tilde{B}_y}$ near the Γ point with $\theta_s = \pi/4$ and $3\pi/4$, respectively, where n takes the highest valence band, m takes the lowest conductance band, and the unit is $-de/\hbar$. The dashed curve shows the equal energy contour for the optical transition with different photon energy (in units of M_1). (e) The geometrical peak of λ as a function of θ_s, fitted to the function $\alpha_1 \sin(2\theta_s)$. (f) A schematic plot of the strain-tunable NDD device setup. Pink and yellow arrows represent interlayer antiferromagnetic order, and the incident and transmitted light, respectively.

Third, in experiments the NDD is generally probed by measuring the difference in the transmitted light with the same incident power but opposite propagation directions. The resulting NDD coefficient is usually defined as $\chi = \{[|\boldsymbol{E}_{\rm out}(q_z)|^2 - |\boldsymbol{E}_{\rm out}(-q_z)|^2]/[(|\boldsymbol{E}_{\rm out}(q_z)|^2 + |\boldsymbol{E}_{\rm out}(-q_z)|^2)/2]\}$. By using electrodynamic theory, one can obtain [39]

$$\chi = -2\mu_0\omega \mathrm{Re}[\sigma_{xxz}(\omega)], \tag{7}$$

where μ_0 is the vacuum permeability. Equation (7) directly relates NDD to the higher-order optical conductivity $\sigma_{xxz}(\omega)$ and therefore indicates the mixed Berry curvature as its microscopic origin.

Strain-tunable NDD in the lattice model of bilayer $MnBi_2Te_4$.—To reflect the geometrical features of NDD, we take a generic lattice model [13,41] with magnetic point group $\bar{3}'m'$ as a concrete example [the structure is shown in Fig. 1(a)]. It can represent bilayer antiferromagnets such as $MnBi_2Te_4$ [42]. Although both $\mathcal{T}$ and $\mathcal{I}$ symmetries are broken, which fulfills the spatial temporal symmetry requirement of NDD, the appearance of C_{2x} symmetry $(x \to x, y \to -y, z \to -z)$ forbids $\sigma_{xxz}(\omega)$ and hence a NDD, based on Eq. (1). This is also confirmed from our calculation. By applying an in-plane uniaxial strain [39], the C_{2x} symmetry is generally broken, and the NDD then emerges. In Fig. 1(b), we plot the NDD signal per unit thickness (black curve) defined as $\lambda = (\chi/2d)$, with the strain being applied along the direction making a $\theta_s = \pi/4$ angle with the x axis. We find that λ has two peaks at $\hbar\omega = 3M_1$ and $8.5M_1$, respectively. Here, M_1 is a parameter of the lattice model [39].

Optical signals are generally related to the joint density of states (JDOS), which is defined as

$$\mathrm{JDOS} = \mathrm{Im}\sum_{m\neq n}\int \frac{d\boldsymbol{k}}{(2\pi)^2}\frac{f_{mn}}{\varepsilon_{mn} - \hbar\omega - i\eta}, \tag{8}$$

which represents the number of the initial and final states in the optical transition. By comparing the JDOS (red curve) and λ in Fig. 1(b), we show that the peak at $\hbar\omega = 8.5M_1$ is indeed due to the JDOS.

The first peak at $\hbar\omega = 3M_1$ is of pure geometrical origin. Based on Eq. (2), both the number of states and the mixed Berry curvature contribute to NDD. We can then isolate the latter by considering the averaged Berry curvature in the optical transition defined as λ/JDOS, as shown in Fig. 1(b) (blue curve). It shows the same two peaks with opposite relative peak strength compared to λ, clearly showing the essential role of the mixed Berry curvature at the first peak.

To further understand the large peak in λ/JDOS around $\hbar\omega = 3M_1$, we plot the distribution of the Berry curvature

near the Γ point in Fig. 1(c). The background Berry curvature at zero strain is subtracted as it does not contribute to the NDD signal. We find that the Berry curvature has a hot spot area inside $\hbar\omega = 3M_1$. Together with the increasing weight factor ε_{mn}^2 in Eq. (2), the peak is then shifted toward the blue side around $3M_1$.

Remarkably, the distribution of the mixed Berry curvature is strongly tied to the strain direction. In Fig. 1(d), we plot the Berry curvature distribution with the strain direction $\theta_s = 3\pi/4$. Comparing Figs. 1(c) and 1(d), we find that the hot spot area of the Berry-curvature distribution changes drastically. Moreover, we note that by a C_{2x} operation, the strain with $\theta_s = \pi/4$ changes to that with $\theta_s = 3\pi/4$. The mixed Berry curvature $\Omega^{nm}_{k_x,\tilde{B}_y}$ flips sign under C_{2x} due to the $\tilde{B}_y$ derivative. As a result, by flipping the distribution of the Berry curvature according to C_{2x} in Fig. 1(c) and interchanging the red and blue color, we obtain Fig. 1(d).

Such a close relation between Berry curvature and strain leads to a highly tunable NDD. Figure 1(e) plots the geometrical peak of λ as a function of the strain angle. One can see that both the amplitude and sign of the NDD signal can be tuned by varying the strain direction. This is in accordance with the C_{2x} symmetry: The strain with $\theta_s = \theta_0$ is related to that with $\theta_s = \pi - \theta_0$, and the resulting NDD signal is odd under C_{2x} and hence changes sign. The magnitude of the NDD has to change, since at $\theta_s = 0$ and $\pi/2$, the C_{2x} symmetry is restored and the NDD signal vanishes. In fact, λ fits the function $\alpha_1 \sin(2\theta_s)$ very well. Since $\boldsymbol{q} \times \boldsymbol{E} = \omega \boldsymbol{B}$, the response coefficient $\sigma_{xxz}(\omega)$ is a component of a rank-two tensor β_{ij} with $J_i = \beta_{ij} B_j$ and $\sigma_{xxz}(\omega) = \beta_{xy}/\omega$. The C_{2x} symmetry forbids β_{xy} without strain. With strain, β_{ij} becomes nonzero and has the general form of $\beta_{ij} = \gamma_{ijk\ell} S_{k\ell}$ with $S_{k\ell}$ being the strain. $\gamma_{ijk\ell}$ is hence a rank-four tensor, and the point-group symmetry imposes the constraint $\gamma_{ijk\ell} = \det(R) R_{i'i} R_{j'j} R_{k'k} R_{\ell'\ell} \gamma_{i'j'k'\ell'}$ with R_{ij} being the transformation matrix. By setting $i = x$ and $j = y$, one can find that only two components are nonzero [39], i.e., $\gamma_{xyxy} = \gamma_{xyyx}$. At fixed strain strength S_0, the response coefficient has the form

$$\beta_{xy} = \beta_0 S_0 \sin(2\theta_s), \tag{9}$$

where $\beta_0 = \gamma_{xyxy}$. This agrees well with the numerical result as displayed in Fig. 1(e).

Based on the above analysis, one can design the device setup for NDD in $MnBi_2Te_4$ as displayed in Fig. 1(f). By varying the strain direction, one can then obtain the favorable propagation direction of light. Moreover, we reveal the dependence of the NDD signal λ on various model parameters and estimate that λ can vary from 10 to 10^3 m^{-1} [39], which is well within the experimental measurable range [25,27,30].

Magnetic quadrupole of wave packet.—The NDD in two-dimensional antiferromagnets has a distinct macroscopic origin. In three dimensions, previous experiments have shown that NDD is a sensitive probe of the multiferroic order $\boldsymbol{P} \times \boldsymbol{M}$ or the antiferromagnetic order with either a spin toroidal moment $\boldsymbol{t}$ or a spin magnetic quadrupole moment q^s_{ij}. However, none of them is responsible for the NDD in bilayer $MnBi_2Te_4$ with strain. First, the in-plane uniaxial strain does not break the combined $\mathcal{TI}$ symmetry. Therefore, both $\boldsymbol{P}$ and $\boldsymbol{M}$ are vanishing, as well as $\boldsymbol{P} \times \boldsymbol{M}$. Second, with strain, the lattice sites on different layers move in the same way inside the layer with their distance along the thickness direction unchanged. Since the spin orders on different layers are antiparallel, one immediately finds that $\boldsymbol{t}$ and the off-diagonal elements of q^s_{ij} are zero, while the diagonal elements of q^s_{ij} are nonzero but unchanged. They cannot explain the sensitive dependence of NDD on strain, as discussed previously.

Other than the spin toroidal moment and the spin quadrupole moment due to the spin texture within a unit cell, there is a different definition of the spin magnetic quadrupole labeled as $\mathcal{Q}_{ij}$ [43], which is for the wave packet of Bloch electrons. It is consistent with the $\mathcal{TI}$ symmetry and is a secondary order parameter associated with the antiferromagnetism as well. Its formal definition reflects the free energy response with respect to a nonuniform magnetic field and its microscopic expression is written as [39]

$$\mathcal{Q}_{ij} = \int_{\mathrm{BZ}} \frac{d\boldsymbol{k}}{(2\pi)^2} \sum_{n \in \mathrm{occ}} \left\{ -\frac{g\mu_B}{\hbar} \sum_{n \neq m} \mathrm{Re}(A^i_{nm} s^j_{mn}) + (\varepsilon_n - \mu) \Omega^n_{k_i,\tilde{B}_j} \right\}, \tag{10}$$

where g is the gyromagnetic factor, μ_B is the Bohr magneton, μ is the chemical potential, $\boldsymbol{A}_{nm} = \langle n\boldsymbol{k}|i\partial_{\boldsymbol{k}}|m\boldsymbol{k}\rangle$ is the Berry connection, and $\boldsymbol{s}_{mn} = \langle m\boldsymbol{k}|\hat{\boldsymbol{s}}|n\boldsymbol{k}\rangle$ is the spin matrix element.

Such a magnetic quadrupole can be analogous to the orbital magnetization [54,55]. In Eq. (10), by changing $-g\mu_B \hat{\boldsymbol{s}}/\hbar$ to the current operator $-e\hat{\boldsymbol{v}}$ in the first term and $\Omega^n_{k_i,\tilde{B}_j}$ to $-(e/\hbar)\Omega^n_{k_i,k_j}$ in the second term, one can recover the familiar expression for the orbital magnetization. Similar to the orbital magnetic moment from the self-rotation of the wave packet in the orbital magnetization, the first term in Eq. (10) can be considered as the spin texture within a wave packet. The second term in Eq. (10) is due to the spin polarization on the boundary: There is a confining potential V near the boundary, whose gradient ∇V yields an electric field. Based on the magnetoelectric coupling, such an electric field then generates a spin magnetization on the boundary, corresponding to the center-of-mass spin magnetization of the wave packet and then leading to an additional contribution to the magnetic quadrupole. This physical picture is similar to the boundary current contribution to the orbital magnetization.

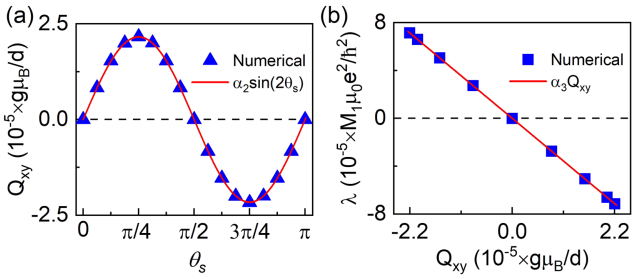

FIG. 2. The magnetic quadrupole for the NDD. (a) The strain angle θ_s dependence of the magnetic quadrupole $\mathcal{Q}_{xy}$. (b) The NDD signal against the magnetic quadrupole $\mathcal{Q}_{xy}$.

The mutual dependence of $\mathcal{Q}_{xy}$ and $\sigma_{xxz}(\omega)$ on the mixed Berry curvature indicates that $\mathcal{Q}_{xy}$ is the macroscopic order parameter sensed by NDD. This can be further confirmed by utilizing the close relation between mixed Berry curvature and the strain. At zero strain, $\mathcal{Q}_{xy}$ vanishes identically, just as NDD. Figure 2(a) plots $\mathcal{Q}_{xy}$ against the strain angle. One finds that it exhibits a sinusoidal profile similar to NDD in Fig. 1(e). By directly plotting the NDD against $\mathcal{Q}_{xy}$ at different strain angles as displayed in Fig. 2(b), one can find that the NDD is indeed linearly correlated to $\mathcal{Q}_{xy}$.

In summary, we show the mixed Berry curvature as the geometrical origin of the NDD for two-dimensional antiferromagnets. It is closely related to the uniaxial strain, offering a highly tunable NDD. Such a close relation between Berry curvature and strain also reveals the magnetic quadrupole of the wave packet as the macroscopic order parameter for NDD in two dimensions, which is distinct from the multiferroic order $\boldsymbol{P}\times\boldsymbol{M}$ or the spin toroidal and quadrupole order in three dimensions. Finally, we emphasize that our numerical results based on the lattice mode hold in a family of two-dimensional antiferromagnets with the same magnetic point group, such as $EuBi_2Te_4$ [13], $MnSb_2Te_4$ [13], CrI_3 [56], etc.

Y. G. is supported by the National Key R&D Program (Grant No. 2022YFA1403502) and Fundamental Research Funds for the Central Universities (Grant No. WK2340000102). W. L. and Z. Q. are supported by the National Natural Science Foundation of China (Grants No. 11974327 and No. 12004369), Natural Science Basic Research Program of Shanxi (No. 20210302124252), Anhui Initiative in Quantum Information Technologies (Grant No. AHY170000), and the Innovation Program for Quantum Science and Technology (Grant No. 2021ZD0302800). J. Z. is supported by the National Natural Science Foundation of China (Grant No. 12247181). Q. N. is supported by the National Natural Science Foundation of China (Grant No. 12234017). We also thank the Supercomputing Center of University of Science and Technology of China for providing the high-performance computing resources.

*Corresponding author: qiao@ustc.edu.cn
†Corresponding author: ygao87@ustc.edu.cn

[1] B. Huang, G. Clark, E. Navarro-Moratalla, D. R. Klein, R. Cheng, K. L. Seyler, D. Zhong, E. Schmidgall, M. A. McGuire, D. H. Cobden *et al.*, Nature (London) **546**, 270 (2017).
[2] B. Huang, G. Clark, D. R. Klein, D. MacNeill, E. Navarro-Moratalla, K. L. Seyler, N. Wilson, M. A. McGuire, D. H. Cobden, D. Xiao *et al.*, Nat. Nanotechnol. **13**, 544 (2018).
[3] W. Chen, Z. Sun, Z. Wang, L. Gu, X. Xu, S. Wu, and C. Gao, Science **366**, 983 (2019).
[4] Z. Sun, Y. Yi, T. Song, G. Clark, B. Huang, Y. Shan, S. Wu, D. Huang, C. Gao, Z. Chen *et al.*, Nature (London) **572**, 497 (2019).
[5] V. Baltz, A. Manchon, M. Tsoi, T. Moriyama, T. Ono, and Y. Tserkovnyak, Rev. Mod. Phys. **90**, 015005 (2018).
[6] S. Rahman, J. F. Torres, A. R. Khan, and Y. Lu, ACS Nano **15**, 17175 (2021).
[7] L. Šmejkal, Y. Mokrousov, B. Yan, and A. H. MacDonald, Nat. Phys. **14**, 242 (2018).
[8] P. Němec, M. Fiebig, T. Kampfrath, and A. V. Kimel, Nat. Phys. **14**, 229 (2018).
[9] K. S. Novoselov, A. Mishchenko, A. Carvalho, and A. H. Castro Neto, Science **353**, aac9439 (2016).
[10] K. S. Novoselov, D. Jiang, F. Schedin, T. J. Booth, V. V. Khotkevich, S. V. Morozov, and A. K. Geim, Proc. Natl. Acad. Sci. U.S.A. **102**, 10451 (2005).
[11] S. Manzeli, D. Ovchinnikov, D. Pasquier, O. V. Yazyev, and A. Kis, Nat. Rev. Mater. **2**, 17033 (2017).
[12] Y. Liu, N. O. Weiss, X. Duan, H.-C. Cheng, Y. Huang, and X. Duan, Nat. Rev. Mater. **1**, 16042 (2016).
[13] D. Zhang, M. Shi, T. Zhu, D. Xing, H. Zhang, and J. Wang, Phys. Rev. Lett. **122**, 206401 (2019).
[14] C. Liu, Y. Wang, H. Li, Y. Wu, Y. Li, J. Li, K. He, Y. Xu, J. Zhang, and Y. Wang, Nat. Mater. **19**, 522 (2020).
[15] J. Li, Y. Li, S. Du, Z. Wang, B.-L. Gu, S.-C. Zhang, K. He, W. Duan, and Y. Xu, Sci. Adv. **5**, eaaw5685 (2019).
[16] W. Liang, T. Hou, J. Zeng, Z. Liu, Y. Han, and Z. Qiao, Phys. Rev. B **107**, 075303 (2023).
[17] S. Du, P. Tang, J. Li, Z. Lin, Y. Xu, W. Duan, and A. Rubio, Phys. Rev. Res. **2**, 022025(R) (2020).
[18] C.-P. Zhang, X.-J. Gao, Y.-M. Xie, H. C. Po, and K. T. Law, Phys. Rev. B **107**, 115142 (2023).
[19] R. Chen, H.-P. Sun, M. Gu, C.-B. Hua, Q. Liu, H.-Z. Lu, and X. C. Xie, Natl. Sci. Rev. nwac140 (2022).
[20] A. Gao, Y.-F. Liu, C. Hu, J.-X. Qiu, C. Tzschaschel, B. Ghosh, S.-C. Ho, D. Bérubé, R. Chen, H. Sun *et al.*, Nature (London) **595**, 521 (2021).
[21] R. Fuchs, Philos. Mag. **11**, 647 (1965).
[22] Y. Gao and D. Xiao, Phys. Rev. Lett. **122**, 227402 (2019).
[23] J. Goulon, A. Rogalev, C. Goulon-Ginet, G. Benayoun, L. Paolasini, C. Brouder, C. Malgrange, and P. A. Metcalf, Phys. Rev. Lett. **85**, 4385 (2000).

[24] S. Toyoda, N. Abe, S. Kimura, Y. H. Matsuda, T. Nomura, A. Ikeda, S. Takeyama, and T. Arima, Phys. Rev. Lett. **115**, 267207 (2015).
[25] M. Kubota, T. Arima, Y. Kaneko, J. P. He, X. Z. Yu, and Y. Tokura, Phys. Rev. Lett. **92**, 137401 (2004).
[26] Y. Tokura and N. Nagaosa, Nat. Commun. **9**, 3740 (2018).
[27] I. Kezsmarki, N. Kida, H. Murakawa, S. Bordacs, Y. Onose, and Y. Tokura, Phys. Rev. Lett. **106**, 057403 (2011).
[28] Y. Okamura, F. Kagawa, M. Mochizuki, M. Kubota, S. Seki, S. Ishiwata, M. Kawasaki, Y. Onose, and Y. Tokura, Nat. Commun. **4**, 2391 (2013).
[29] Y. Takahashi, R. Shimano, Y. Kaneko, H. Murakawa, and Y. Tokura, Nat. Phys. **8**, 121 (2011).
[30] J. H. Jung, M. Matsubara, T. Arima, J. P. He, Y. Kaneko, and Y. Tokura, Phys. Rev. Lett. **93**, 037403 (2004).
[31] Y. Shimada, M. Matsubara, Y. Kaneko, J. P. He, and Y. Tokura, Appl. Phys. Lett. **89**, 101112 (2006).
[32] M. Saito, K. Taniguchi, and T. Arima, J. Phys. Soc. Jpn. **77**, 013705 (2008).
[33] I. Kézsmárki, U. Nagel, S. Bordács, R. S. Fishman, J. H. Lee, H. T. Yi, S.-W. Cheong, and T. Rõõm, Phys. Rev. Lett. **115**, 127203 (2015).
[34] T. Sato, N. Abe, S. Kimura, Y. Tokunaga, and T. Arima, Phys. Rev. Lett. **124**, 217402 (2020).
[35] K. Kimura, Y. Otake, and T. Kimura, Nat. Commun. **13**, 697 (2022).
[36] Y. Sawada, S. Kimura, K. Watanabe, Y. Yamaguchi, T. Arima, and T. Kimura, Phys. Rev. Lett. **129**, 217201 (2022).
[37] K. Sawada and N. Nagaosa, Phys. Rev. Lett. **95**, 237402 (2005).
[38] N. A. Spaldin, M. Fiebig, and M. Mostovoy, J. Phys. Condens. Matter **20**, 434203 (2008).
[39] See Supplemental Material at http://link.aps.org/supplemental/10.1103/PhysRevLett.131.256901 for the derivation of (i) Eqs. (2), (3), (5), (6), (7), (9), and (10); (ii) the tight-binding model; (iii) the uniaxial strain and the estimation of the NDD signal strength; (iv) the dependence of NDD signal on different material properties; (v) the optical conductivity of general multilayer systems that are amenable for first-principles calculations, which includes Refs. [13,40–52].
[40] T. Stauber, T. Low, and G. Gómez-Santos, Phys. Rev. B **98**, 195414 (2018).
[41] R. X. Zhang, F. Wu, and S. Das Sarma, Phys. Rev. Lett. **124**, 136407 (2020).
[42] H. Wang and X. Qian, npj Comput. Mater. **6**, 199 (2020).
[43] Y. Gao, D. Vanderbilt, and D. Xiao, Phys. Rev. B **97**, 134423 (2018).
[44] M. P. Marder, *Condensed Matter Physics* (John Wiley & Sons, New York, 2010).
[45] H.-P. Sun, C. M. Wang, S.-B. Zhang, R. Chen, Y. Zhao, C. Liu, Q. Liu, C. Chen, H.-Z. Lu, and X. C. Xie, Phys. Rev. B **102**, 241406(R) (2020).
[46] B. Aslan, M. Deng, and T. F. Heinz, Phys. Rev. B **98**, 115308 (2018).
[47] A. Davydov, K. Choo, M. H. Fischer, and T. Neupert, Phys. Rev. B **105**, 165153 (2022).
[48] M. Koshino and N. N. T. Nam, Phys. Rev. B **101**, 195425 (2020).
[49] M. Kubota, T. Arima, Y. Kaneko, J. P. He, X. Z. Yu, and Y. Tokura, Phys. Rev. Lett. **92**, 137401 (2004).
[50] J. H. Jung, M. Matsubara, T. Arima, J. P. He, Y. Kaneko, and Y. Tokura, Phys. Rev. Lett. **93**, 037403 (2004).
[51] I. Kézsmárki, N. Kida, H. Murakawa, S. Bordács, Y. Onose, and Y. Tokura, Phys. Rev. Lett. **106**, 057403 (2011).
[52] A. Authier, *International Tables for Crystallography, Volume D: Physical Properties of Crystals* (Kluwer Academic Publishers, Dordrecht, 2003).
[53] I. Souza and D. Vanderbilt, Phys. Rev. B **77**, 054438 (2008).
[54] D. Xiao, M.-C. Chang, and Q. Niu, Rev. Mod. Phys. **82**, 1959 (2010).
[55] D. Ceresoli, T. Thonhauser, D. Vanderbilt, and R. Resta, Phys. Rev. B **74**, 024408 (2006).
[56] N. Sivadas, S. Okamoto, X. Xu, C. J. Fennie, and D. Xiao, Nano Lett. **18**, 7658 (2018).